Aperiodic spin state ordering of bistable molecules and its photoinduced erasing

Eric Collet, Hiroshi Watanabe, Nicolas Bréfuel, Lukas. Palatinus, Ludovic Roudaut, Loïc Toupet, Koichiro Tanaka, Jean-Pierre Tuchagues, Pierre Fertey, Sylvain Ravy, et al.

Aperiodic spin state ordering of bi-stable molecules and its photoinduced erasing

E. Collet,[1,a] H. Watanabe,[1] N. Bréfuel,[2] L. Palatinus,[3] L. Roudaut,[1] L. Toupet,[1] K. Tanaka,[4] J.-P. Tuchagues,[5] P. Fertey,[6] S. Ravy,[6] B. Toudic,[1] H. Cailleau[1]

[1] *Institut de Physique de Rennes, Université de Rennes I - CNRS, UMR 6251, F-35 042 Rennes.*

[2] *Laboratoire National des Champs Magnétiques Intenses, UPR 3228, F-38042 Grenoble cedex 9.*

[3] *Department of Structure Analysis, Institute of Physics of Academy of Sciences of Czech Republic, Cz-182 21 Prague.*

[4] *Institute for Integrated Cell-Material Sciences, Kyoto University, Sakyo-ku, KyotoJ- 606-8501, and CREST, Japan Science and Technology Agency, Kawaguchi, Saitama J-332 0012*

[5] *Laboratoire de Chimie de Coordination and Université de Toulouse, UPR-CNRS 8241 205, F-31077 Toulouse.*

[6] *Synchrotron SOLEIL, L'Orme des Merisiers, Saint Aubin - B.P. 48, F-91 192 Gif-sur-Yvette.*

We describe a novel type of ordering phenomenon associated with the incommensurate occupational modulation of bistable molecular magnetic states in a spin-crossover material. This unusual type of aperiodicity resulting from the ordering of multi-stable electronic states opens new possibilities for addressing such materials by light. Here we show that light can switch the crystal from 4D to 3D periodic structure. Mixing aperiodicity, multi-stability and photoinduced phenomena opens new perspectives for directing complex order and function in material science.

PACS Codes : 61.44.Fw, 64.70.Rh, 75.30.Wx, 82.50.Hp

The control of the functionality of a material requires understanding the complex organization of its atomic or electronic constituents, but also understanding the bi-stable or multi-stable processes addressable by external stimulation, including light for the photo-control[1,2,3,4]. On the one hand, macroscopic ordering is manifested by the appearance of regular patterns, which in some cases never repeat themselves periodically in 3D space but only in a higher dimension space: this so-called aperiodicity[5,6,7] plays a central role in the structure and physical properties of materials as diverse as quasicrystals[8], charge-density[1] and spin-density waves[9,10], or new superconductors[11] for instance. On the other hand, some materials exhibit more or less cooperative switching between bi-stable functional molecular states[12,13,14,15], controllable with temperature, pressure, light… The relationship between molecular bistability in the solid state and aperiodicity has not been considered so far. Here, we describe a novel type of ordering phenomenon associated with the appearance of an incommensurate molecular spin state modulation of a bi-stable spin-crossover compound. It results from a concerted interplay between the symmetry breaking associated with the aperiodic ordering and the thermal balance between the two functional states. Contrary to usual incommensurate composition systems[16,17,18,19], for which the species concentrations are chemically fixed, in bi-stable systems the average concentration of molecular states can fluctuate, evolve and be controlled by external stimuli. And so we show that a laser excitation, selectively populating a single molecular state, can erase the incommensurate phase and switch the crystal structure from 4D to 3D periodic. Mixing aperiodicity, multi-stability and photoinduced phenomena opens new perspectives for directing complex order and function.

Fe(II)-based spin crossover (SC) compounds are prototypic bi-stable molecular systems. Both basic scientific research[20], as well as potential technological applications were investigated, because of ultrafast-switching[21], information storage or visual displays[13,22] abilities. The possibility offered by various external control parameters such as temperature, pressure or light irradiation for balancing the relative population between low-spin (LS, S=0) and high-spin (HS, S=2) states has attracted much interest and many such complexes have been widely studied over the past decades[12]. In addition to simple entropy-driven macroscopic conversion from LS to HS, complex phenomena resulting from the partial spin conversion and the periodic ordering of HS and LS states around stepped transitions have been described[23,24,25,26]. In this paper we describe a novel type of phase, where the long-range order of HS and LS molecular states is incommensurately modulated with respect to the 3D structure. This exotic phase is observed in the new spin crossover material $[Fe^{II}H_2L^{2\text{-}Me}][SbF_6]_2$ ($H_2L^{2\text{-}Me}$ denotes the organic ligand bis[((2-methylimidazol-4-yl)methylidene)-3-aminopropyl] ethylenediamine)[27]. We first describe the features of this novel modulated structure as obtained from a structure analysis in 4D superspace, and then we show that it can be erased by laser irradiation.

The $[Fe^{II}H_2L^{2\text{-}Me}]^{2+}$ cation in complexes is able to switch from HS to LS states when temperature is decreased as demonstrated in salts with PF_6^- or AsF_6^- anions[25,26,28]. The concentration in HS molecules (γ_{HS}) can be accurately measured by different techniques[12]: here we use magnetic susceptibility, Mössbauer spectroscopy and X-ray diffraction

[a] To whom correspondence should be addressed. E-mail: eric.collet@univ-rennes1.fr

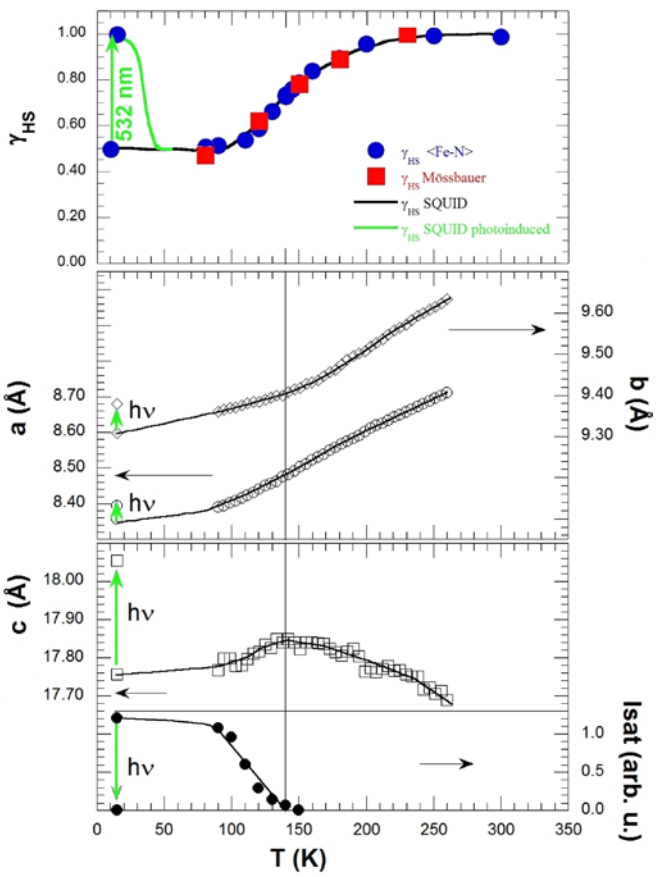

Fig. 1: Temperature dependence of the HS fraction γ_{HS} in the $[Fe^{II}H_2L^{2\text{-}Me}][SbF_6]_2$ complex, extracted from <Fe-N> bond length obtained by X-ray diffraction (●), Mössbauer data (■) and magnetic susceptibility (lines) [27]. Photoinduced spin-state switching is performed at low temperature with 532 nm irradiation. The temperature dependence of the unit cell parameters a (○), b(◊) and c (□) and of the average intensity (●) of few selected satellite reflections indicate a second order transition towards the incommensurate phase around 140 K and a photoinduced transition reached by irradiation at 532 nm (hν) at low temperature.

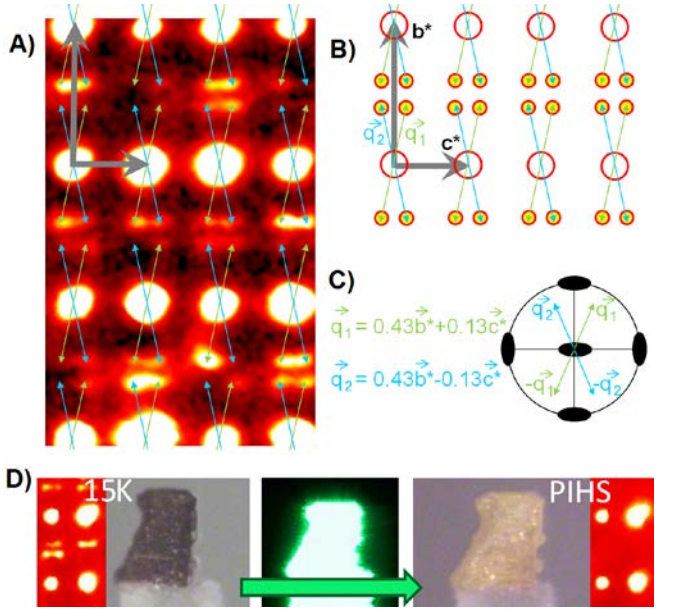

Fig. 2. Satellites reflections in the aperiodic phase : (A) diffracted intensity in the (b*,c*) reciprocal plane, with intense Bragg reflections at the nodes and weak satellites reflections in incommensurate positions observed in the aperiodic phase. (B) Schematic indexation of the reflections with (b*,c*,q_1) or (b*,c*,q_2). (C) Stereographic projection along a of the 4 branches star of k in the 222 symmetry class (2 fold axes are represented by solid ellipses): two types of domains exist each associated to a modulation vector q_1 or q_2. Any reflection is therefore indexed ha*+kb*+lc*+mq_1 or ha*+kb*+lc*+mq_2. D) At 15K in the incommensurate phase with satellite reflections the crystal color is dark purple. In the photoinduced HS state reached after photoexcitation at 532 nm the crystal color is yellow and the satellites reflections disappear, as in the HS state above 250 K.

to study the SbF_6^- complex. Fig. 1 shows the temperature dependence of γ_{HS} estimated from the $\chi_M T$ product (Fig. S1), Mössbauer analysis (Fig. S2 & Tab. S1), and structure analysis by x-ray diffraction (Tab S2 & S3). In this family of complexes, the Fe(II) ion is coordinated by 6 nitrogen atoms of the ligand, in a nearly octahedral field. [29] It is well known that the change of d^6 shell occupancy between LS ($t_{2g}^6 - e_g^0$) and HS ($t_{2g}^4 - e_g^2$) is associated with an elongation of the average <*Fe-N*> bond length.[23,24] For $[Fe^{II}H_2L^{2\text{-}Me}]$ cation in the PF_6 and AsF_6 salts, <*Fe-N*> changes from 2.01 Å (LS) to 2.19 Å (HS).[25,26,28] At room temperature these complexes are isostructural to the reported SbF_6 derivative (space group $P22_12_1$, Fig. S3). When LS and HS states coexist in the crystal, structural analysis allows determining γ_{HS} through its correlation with <*Fe-N*>, as this one is modified by the relative contribution of LS and HS states (Tab. S3).[25-27] Fig. 1 shows that above 230 K γ_{HS}=1, whereas at low temperature, below 90 K, a plateau is reached at γ_{HS}≈0.5. This is characterized by the partial contraction of <*Fe-N*> (2.10 Å, Tab S3), the magnetic susceptibility (Fig. S1) and Mössbauer spectra (Fig. S2). The above-mentioned methods confirm the known agreement of structural analysis based on <*Fe-N*> for determining γ_{HS}, which we use to analyse the aperiodic structure.

X-ray data collected below 150 K revealed new Bragg reflections (Fig. 2, S4 & S5) corresponding to a lowering of symmetry. On the one hand, Bragg reflections characterizing the loss of 2_1 screw axes along **b** and **c** (Fig. S6) indicate a change of the crystalline system from orthorhombic to monoclinic (**a** being the monoclinic axis). On the other hand, other types of numerous weak reflections appear, but cannot be indexed with three basis vectors. As shown in Fig. 2 & S4, a 4 vector basis **a***, **b***, **c*** and **q** must be used. However, because of the symmetry lowering, two types of domains are formed in the star of **k** (Fig. 2c) corresponding to $\mathbf{q}_1$ or $\mathbf{q}_2$ (two directions equivalent in the high-symmetry phase). All these reflections are therefore indexed with the scattering vectors **Q** given by:

$\mathbf{Q}=h\mathbf{a}^* + k\mathbf{b}^* + l\mathbf{c}^* + m\mathbf{q}_1$ or $\mathbf{Q}=h\mathbf{a}^* + k\mathbf{b}^* + l\mathbf{c}^* + m\mathbf{q}_2$ h, k, l & m being integer.

The two modulation vectors correspond to $\mathbf{q}_1 = \beta\mathbf{b}^* + \gamma\mathbf{c}^*$ and $\mathbf{q}_2 = -\beta\mathbf{b}^* + \gamma\mathbf{c}^*$. Since we found that β= 0.431(5) and γ=0.131(5) (Fig. S4), the components of **q** are not simple fractional numbers and thus the structure is incommensurately modulated [5-7]. Only main reflections (m=0) and first-order satellites (m=±1) are observed down to 15 K (Fig. 2 & S4). Reflections indexed by a combination $\mathbf{q}_1 \pm \mathbf{q}_2$ are not observed since the modulated structure is multi-domain single **q** and the direction of the modulation vector corresponds to the decrease in symmetry from orthorhombic to monoclinic. Consequently, during this phase transition the symmetry changes from an orthorhombic ($P22_12_1$) system

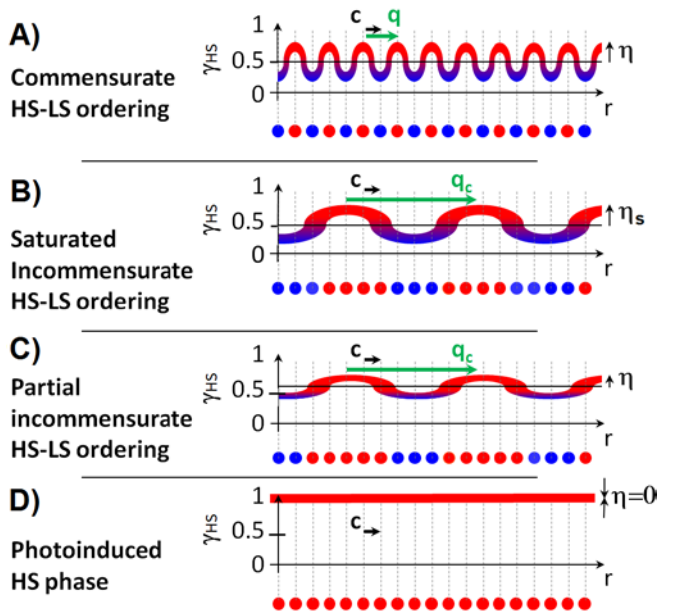

Fig. 3. HS-LS ordering schematically represented by an occupational wave $\gamma_{HS}(r)=\gamma_{HS}+\eta\times\cos(q.r)$. A) commensurate case (q=c*/2) where the periodicity of the modulation is 2c (green) around an average value γ_{HS}=0.5 (line) and with an amplitude η, giving rise to alternation of mainly HS (red) and LS (blue) spin-state occupation over the different molecular sites (spheres) along the c axis. B) incommensurate case projected along c direction (q_c=0.131c*) gives an aperiodic alternation around an average value γ_{HS}=0.5 and with a saturated amplitude η_s. C) intermediate incommensurate case characterized by a larger fraction of HS (red) sites with γ_{HS} >0.5 and an amplitude 0<η<η_s. D) the photoinduced HS phase where γ_{HS} (r)=1 and η the amplitude of the concentration wave vanishes.

with 3D periodic structure to an incommensurately modulated structure with a 4D superspace group symmetry P211(0βγ). The continuous evolution of the satellite reflections around 140 K, concomitant with a change of slope in the temperature dependence of the lattice parameters (Fig. 1), underline the second order nature of the phase transition.

The structure of the incommensurate phase was refined in a (3+1)-dimensional superspace[6]. The detailed description of the structural analysis is given in the supplemental material[27] and we focus here on the main conclusions. The aperiodic structure can be interpreted as resulting from a spatial modulation of the HS fraction, i.e. of the spin-state of the molecules, simply written as:

$$\gamma_{HS}(\mathbf{r})=\gamma_{HS}+\eta\times\cos(\mathbf{q}.\mathbf{r}),$$

where γ_{HS} is the average HS fraction determined in Fig. 1, **q** is the wave vector and η is the amplitude of the wave. In several SC systems, superstructure ordering of γ_{HS} over crystalline sites were reported[23,25], including the isostructural PF_6 derivative[26]. For the latter, the spin-state ordering around an average value of γ_{HS}=0.5 corresponds to a cell doubling along **c** axis, since **q**=**c***/2. Fig. 3a depicts $\gamma_{HS}(\mathbf{r})$, where sites are mainly HS (red) when $\gamma_{HS}(\mathbf{r})$ is above 0.5, or mainly LS (blue) below. We extend this description to the present compound, for which the wavelength of the modulation of $\gamma_{HS}(\mathbf{r})$ around γ_{HS}=0.5 is incommensurate with the average 3D lattice (Fig. 3b). The sequence of HS and LS sites therefore never repeats periodically in the 3D space.

In the full structure model of a modulated structure[20], the atoms must be described by their positions in the average 3D unit cell and by their modulation functions along the fourth dimension coordinate x_4 of the superspace. From the refined superspace structure model, the modulation of <Fe-N> along x_4 can be obtained (Fig. S6 & S7), from which we estimate the amplitude of the modulation to η≈0.37(5) (Fig. 4). The incommensurate spin-state occupation structure can be visualized in the (**b**,**c**) plane in Fig. 4, by using the same colour code as in Figure 3. Clearly, the main character of the modulation is the presence of stripes of HS and LS molecular states, perpendicular to the direction of the modulation vector **q**.

The possibility to control the average concentration of HS molecules by external parameter is an important new aspect with regard to usual incommensurate composition-type systems reported in the literature[5-7,16-19]. For these, the modulation vector can change when the amplitude of the order parameter η evolves with temperature, but the species concentration is chemically fixed. In the present system both the average concentration γ_{HS} and the amplitude η change with temperature but without significant variation of the modulation vector detected. From the temperature dependence of the intensity (Fig. 1) of satellite reflections (in a first approximation $\propto\eta^2$), we can conclude that below 80 K η saturates (around η_s=0.37). These reflections disappearing around 140 K, the amplitude of occupation modulation wave vanishes (η=0) when γ_{HS}≈0.75, i.e. well before 230 K where γ_{HS}=1. An intermediate case corresponding to the 80-140 K range is illustrated in Fig. 3c, where γ_{HS}>0.5 and 0<η<η_s. These data clearly indicate different evolutions of γ_{HS} and η. The appearance of incommensurate structures results from competing interactions over different ranges. In the present case we can mention the competition between long-range elastic interactions and steric effects between the anion and cation layers (Fig. 4), also underlined in the AsF_6 derivative[25] for explaining complex but commensurate spin-states order.

Light is known to be an efficient control parameter in the prototype photoactive SC materials[12,20-22,30], and it was shown for $[Fe^{II}H_2L^{2\text{-}Me}]$ that weak laser irradiation at 532 nm can promote the molecules from LS to HS[25,26,28]. Fig. 1 shows that after few minutes of irradiation at 15 K γ_{HS}=1, as characterized by the values of $\chi_M T$ and <Fe-N > (2.19 Å). This photomagnetic effect is also related here to an important photochromic effect, since the crystal colour changes from dark purple in the incommensurate low temperature phase to yellow in the photoinduced HS and thermal HS phases (Fig. 2), where the satellite reflections disappear. The structure of the photoinduced phase is again 3D periodic, and the disappearance of (0 k 0) and (0 0 l) Bragg reflections with k and l odd shows that the photoinduced phase recovers the orthorhombic $P22_12_1$ symmetry. Except the thermal contraction of the lattice parameters (Fig. 1), the structures of the photoinduced HS and thermal HS phases are identical (Tab S2 & S3). This metastable photoinduced HS state has a lifetime longer than 24h at 15 K once laser excitation is stopped. However, when warmed above 40 K γ_{HS} relaxes back to ≈ 0.5 within few minutes (Fig. 1) and the incommensurate phase is recovered. This behaviour is a proof that it is indeed the spin state which is the primary modulated parameter. When γ_{HS}=1, the spatial modulation of

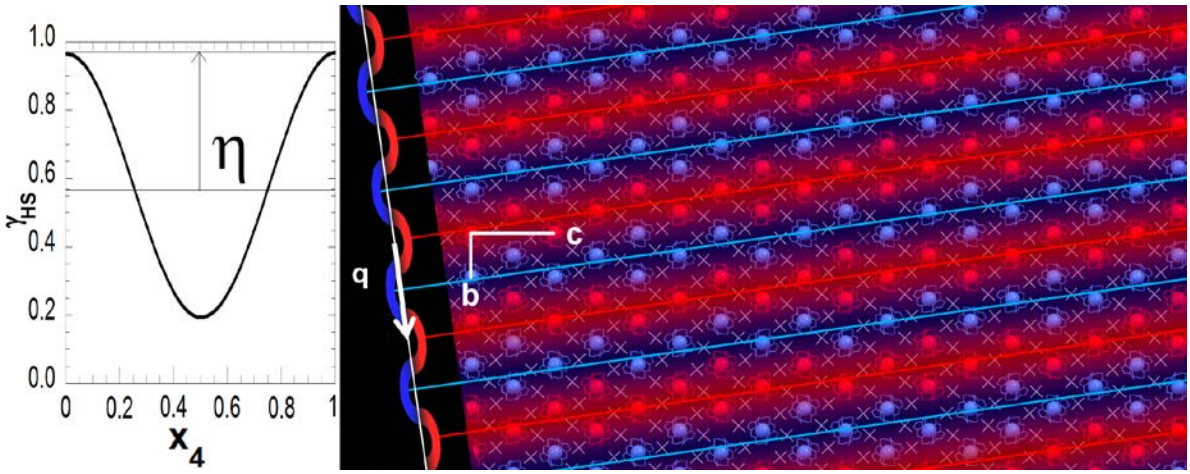

Fig. 4. The aperiodic spin state ordering with the modulation of γ_{HS} along the superspace coordinate x_4 (left), varying between 0.19(5) and 0.94(5), deduced from the modulation of the <Fe-N> bond (Fig. S7). The corresponding structure is projected in 3D space: blue (LS states) and red (HS states) colours schematically reflect the spatial occupation modulation (right). b and c crystalline axes of the average 3D structure are indicated.

$\gamma_{HS}(\mathbf{r})$ vanishes (η=0, Fig. 3d) as only the HS state is occupied over all the crystalline sites.

Our detailed study of the $[Fe^{II}H_2L^{2\text{-}Me}][SbF_6]_2$ material shows that the incomplete conversion of bi-stable molecules is associated with an incommensurate spatial modulation of the molecular spin-state and a description of the structure is obtained in (3+1)-dimensional superspace. The particularity of the present material is that, unlike conventional modulated crystals with occupational, positional or conformational modulation, the primary modulated parameter is the spin-state of bi-stable molecules. As such, this aperiodic structure is demonstrated to be erased by selective laser population of a single molecular state (HS).

With the development of scientific instrumentation, it appears that aperiodicity is ubiquitous in all type of materials. It is therefore very likely that the present concept of aperiodic ordering of molecular state may be applied to other types of photo-active materials exhibiting molecular bi-stability or multi-stability. By crossing the borders between aperiodicity, multi-stability and photoinduced phenomena we have shown that new perspectives appear for switching between different regimes of periodicity and for exploring new phases of matter related to function, such as photochromism and photomagnetism.

This work was supported by the Institut Universitaire de France, Rennes Métropole, Région Bretagne (CREATE Ultimate 4146), the ANR (09-BLAN-0212) and Europe (FEDER). H.W. thanks University Rennes 1 for PD funding. L.R. thanks CNRS for PhD funding.

1 M. Chollet *et al*, *Science* **307**, 86-89 (2005).

2 M. Eichberger *et al*. *Nature* **468**, 799–802 (2010).

3 T. Kosa *et al*, *Nature* **485**, 347–349 (2012)

4 E. Collet *et al*, *Science*, **300**, 612 – 615 (2003)

5 T. Janssen, G. Chapuis, M. de Boissieu, *Aperiodic Crystals: From Modulated Phases to Quasicrystals* (Oxford Univ. Press, Oxford, 2007).

6 S. van Smaalen, *Incommensurate Crystallography* (Oxford Univ. Press, Oxford, 2007).

7 A. Janner, T. Janssen, J.C. Toledano, *Lecture Notes in Physics*, **201**, 364-396 (1984).

8 D. Shechtman, I. Blech, D. Gratias, J. Cahn, *Phys. Rev. Lett.*, **53**, 1951 (1984).

9 B. J. Klemme *et al*, *Phys. Rev. Lett.* **75**, 2408–2411 (1995).

10 G. Grüner, *Density Waves in Solids* (Frontiers in Physics Vol. 89 Addison-Wesley, Reading, MA, 1994).

11 F. Laliberté *et al*, *Nature Com.* **2**, 423 (2011).

12 A. Bousseksou, G. Molnar, L. Salmon, W. Nicolazzi, *Chem. Soc. Rev.*, **40**, 3313-3335 (2011).

13 O. Kahn, C.J. Martinez, *Science* **279**, 44–48 (1998).

14 M. Verdaguer, *Science* **272**, 698–699 (1996).

15 S. Kobatake *et al*, *Nature* **446**, 778–781 (2007).

16 A. Arakcheeva, G. Chapuis, *Acta Cryst.* **B62**, 52–59 (2006).

17 J.M. Perez-Mato *et al*, *J. Mater. Chem.* **9**, 2795-2807 (1999).

18 D. Kucharczyk, W. A. Paciorek, *Acta Cryst.* **A41**, 466-469(1985).

19 R. Blinc, A. P. Levanyuk, *Incommensurate phases in dielectrics.* (Elsevier Science & Technology, 1986)

20 S. Ohkoshi *et al*, *Nature Chem.* **3**, 564-569 (2011).

21 R. Bertoni *et al*, *Angew. Chem. Int. Ed.* **51**, 7485-7489 (2012).

22 J.-F. Létard, *J. Mat. Chem.* **16**, 2550-2559 (2006).

23 D. Boinnard *et al*, *Inorg. Chem.* **33**, 271–281 (1994).

24 S. Bonnet *et al*, *Chem. Commun.* 5619–5621 (2008).

25 N. Bréfuel *et al*, *Chem. Eur. J.* **16**, 14060-14068 (2010).

26 N. Bréfuel *et al*, *Ang. Chem. Int. Ed.* **48**, 304-9307 (2009).

27 See EPAPS Document No. [] for methods and additional data.

28 H. Watanabe *et al*, *Eur. J. Inorg. Chem* (2012), DOI: 10.1002/ejic.2012008786.

29 M. Buron *et al*, *Phys. Rev. B* **85**, 064114 (2012).

30 A. Hauser, J. Adler, P. Gütlich, *Chem. Phys. Lett.* **152**, 468, (1988).

Supporting Online Material for

Aperiodic spin state ordering of bi-stable molecules and its photoinduced erasing

E. Collet,[1,*] H. Watanabe,[1] N. Bréfuel,[2] L. Palatinus,[3] L. Roudaut,[1] L. Toupet,[1] K. Tanaka,[4] J.-P. Tuchagues,[5] P. Fertey,[6] S. Ravy,[6] B. Toudic,[1] H. Cailleau[1]

[1] *Institut de Physique de Rennes, Université de Rennes I - CNRS, UMR 6251, F-35 042 Rennes.*
[2] *Laboratoire National des Champs Magnétiques Intenses, UPR 3228, F-38042 Grenoble cedex 9.*
[3] *Institute of Physics of the Academy of Sciences of the Czech Republic, Cz-182 21 Prague.*
[4] *Institute for Integrated Cell-Material Sciences, Kyoto University, Sakyo-ku, KyotoJ- 606-8501,*
[5] *LCC and Université de Toulouse, UPR-CNRS 8241 205, F-31077 Toulouse.*
[6] *Synchrotron SOLEIL, L'Orme des Merisiers, Saint Aubin - B.P. 48, F-91 192 Gif-sur-Yvette.*

* To whom correspondence should be addressed. E-mail: eric.collet@univ-rennes1.fr

This PDF file includes: Materials, methods and characterization and Figs. S1 to S7 and Tab. S1 to S4.

Synthesis of the $[Fe^{II}H_2L^{2\text{-}Me}][SbF_6]_2$ complex.

The $[Fe^{II}H_2L^{2\text{-}Me}][SbF_6]_2$ complex, in which $H_2L^{2\text{-}Me}$ denotes the ligand bis[((2-methylimidazol-4-yl)methyl idene)-3-aminopropyl] ethylenediamine) was prepared through anaerobic reaction of freshly synthesized $H_2L^{2\text{-}Me}$ Schiff base ligand, with $Fe^{II}Cl_2 \bullet 4H_2O$ in ethanol followed by anion metathesis with $NaSbF_6$, adapted from previous procedure[25,26]. The $[Fe^{II}H_2L^{2\text{-}Me}][SbF_6]_2$ composition was established through CHN elemental analysis.

Magnetic study of the $[Fe^{II}H_2L^{2\text{-}Me}][SbF_6]_2$ complex.

The $\chi_M T$ versus T plot depicted in Figure S1, indicates that this complex exhibits a partial reversible spin crossover. The temperature dependence is the same in the warming and cooling modes. Above 200 K, the saturated $\chi_M T$ value of $(\chi_M T)_{HS} \approx 3.8$ cm^3 mol^{-1} K corresponds to the HS state (S = 2). Upon cooling the sample, $\chi_M T$ gradually decreases in the 200-90 K range, and reaches a plateau (≈ 2.1 cm^3 mol^{-1} K) below 80 K. This $\chi_M T$ value roughly corresponds to 55% of the value observed in the HS state, suggesting that the HS fraction reaches $\gamma_{HS} \approx 0.55$ below 80K (Fig. 1). The decrease of $\chi_M T$ below 15 K is known to be associated with zero field splitting. The LS state being diamagnetic, γ_{HS} was estimated from the $\chi_M T$ product as: $\chi_M T = \gamma_{HS}(T) * (\chi_M T)_{HS}$.

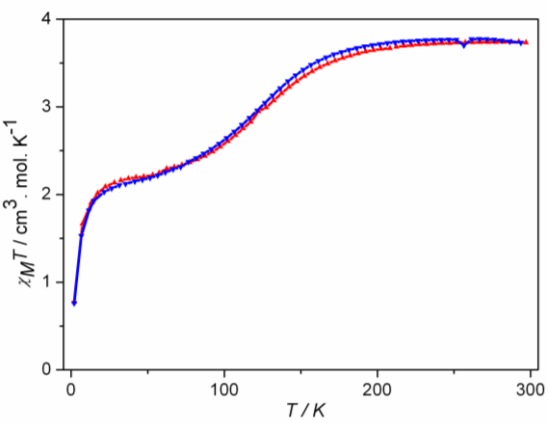

Figure S1. $\chi_M T$ versus T plots of $[Fe^{II}H_2L^{2\text{-}Me}][SbF_6]_2$ measured upon warming the sample from 5 to 300 K at a sweeping rate of 2 K min^{-1} (▲). $\chi_M T$ was then measured upon cooling the sample from 300 to 5 K at the same sweeping rate (▼).

Mössbauer spectroscopy study of the $[Fe^{II}H_2L^{2\text{-}Me}][SbF_6]_2$ complex.

Selected Mössbauer spectra are shown in Figure S2. Table 1S collates the Mössbauer parameters at each selected temperature. At 230 K, the spectrum consists of a unique doublet assigned to the HS Fe^{II} state. Upon decreasing the temperature of the sample from 180 to 120 K, the relative intensity of the HS Fe^{II} doublet decreases, while the LS Fe^{II} doublet increases. At 80 K, the spectrum consists of two doublets assigned to HS Fe^{II} (δ = 1.084(8) mm s^{-1}, ΔE_Q = 1.98(2) mm s^{-1}) and LS Fe^{II} (δ = 0.567(5) mm s^{-1} and ΔE_Q = 0.11(3) mm s^{-1}), pointing to γ_{HS}≈47(3)%.

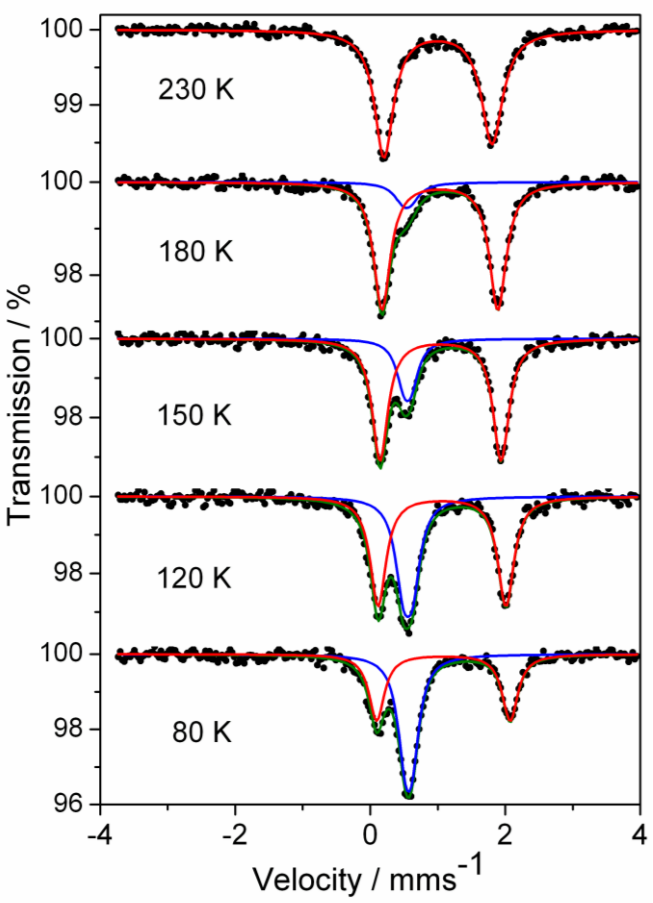

Figure S2. Selected ^{57}Fe Mössbauer spectra of the $[Fe^{II}H_2L^{2\text{-}Me}][SbF_6]_2$ complex recorded at 80, 120, 150, 180 and 230 K upon warming the sample from 80 K. The red curve is a fit of the HS Fe state and the blue one of the LS Fe state.

T / K	δ (LS)	ΔE_Q(LS)	Γ (LS)	% (LS)	δ (HS)	ΔE_Q(HS)	Γ (HS)	% (HS)
80	0.567(5)	0.11(3)	0.13(2)	53(3)	1.084(8)	1.98(2)	0.14(1)	47(3)
120	0.559(8)	0.11(0)	0.13(1)	38(1)	1.066(1)	1.89(2)	0.147(2)	62(3)
150	0.55(1)	0.11(6)	0.13(3)	22(3)	1.042(5)	1.793(9)	0.141(7)	78(4)
180	0.539(3)	0.1(2)	0.16(9)	11(3)	1.033(5)	1.716(8)	0.150(6)	89(3)
230	-	-	-	-	1.005(4)	1.601(9)	0.191(9)	100

Table S1. Mössbauer data for $[Fe^{II}H_2L^{2\text{-}Me}][SbF_6]_2$ (**3**). Isomer shifts (δ, mm s^{-1}) refer to metallic iron at room temperature; quadrupole splittings (ΔE_Q, mm s^{-1}); Γ = half-width of the lines (mm s^{-1}); statistical standard deviations are given in parentheses.

X-ray crystallography study of the $[Fe^{II}H_2L^{2\text{-}Me}][SbF_6]_2$ complex.

The thermal and photoinduced spin conversions of $[Fe^{II}H_2L_2{}^{\text{-}Me}][SbF_6]_2$ were investigated by X-ray diffraction experiments performed on single crystals with typical sizes around 150×100×50 μm^3. The diffraction experiments were carried out on a Xcalibur 3 four-circle diffractometer (Oxford Diffraction) equipped with a 2D sapphire 3 CCD detector with Mo K_α radiation (λ = 0.71069 Å). Diffraction experiments were also performed at the Cristal beamline of the synchrotron Soleil. The unit cell parameters and the data reduction were obtained with the CrysAlis software from Oxford Diffraction.[28]

T [K]	**250 HS**	**80 Aperiodic**	**15 Aperiodic**	**15 PIHS**
Formula	$FeC_{18}H_{30}N_8Sb_2F_{12}$			
Fw [gmol^{-1}]	885.8176			
Crystal system	Orthorhombic	Monoclinic	Monoclinic	Orthorhombic
Space group	$P22_12_1$	$P211$	$P211$	$P22_12_1$
a [Å]	8.6640(10)	8.3947(2)	8.3565(2)	8.3944(4)
b [Å]	9.5670(10)	9.3791(2)	9.3787(3)	9.3078(4)
c [Å]	17.751(4)	17.8310(3)	17.7563(5)	18.0556(8)
α [°]	90	90.058(5)	90.045(6)	90
V[°]	1471.4(4)	1403.92(5)	1394.95(7)	1410.75(11)
Z (cation/unit cell)	2	2	2	2
F(000)	860	860	860	860
ρ_{calcd} [Mgm^{-3}]	2.00	2.096	2.109	2.085
μ ($Mo_{K\alpha}$) [mm^{-1}]	2.410	2.526	2.542	2.514
θ range [°]	2.7 – 27	2.7 – 27	2.7-27	2.7-27
collected data	20007	5741	5033	9727
unique data	3208	4514	3412	3052
R(int)	0.0372	0.0323	0.0227	0.0271
var. param.	187	371	371	186
obsd. Refl.	2616	4219	3038	2978
R obsd., all	0.0296	0.0285	0.0255	0.0271
Rw obsd., all	0.0393	0.0316	0.0322	0.0265

Table S2. Crystallographic data for $[Fe^{II}H_2L^{2\text{-}Me}][SbF_6]_2$. Although the modulated structures at 80 K and 15 K are monoclinic, their average structures are extremely close to orthorhombic and their refinement as orthorhombic gave similar Fe-N bond lengths given in table S3.

The structures were solved by direct methods with SIR-97[29] and refined against F^2 by full-matrix least-squares techniques using SHELXL-97[30] with anisotropic displacement parameters for all non-hydrogen atoms. Data collection and refinement parameters are summarized in Table S2 and the crystal structure

at 250 K is shown in Fig. S3. The evolution of the HS fraction γ_{HS} was estimated through the evolution of the intra-molecular <Fe-N> average bond length Table S3.

The temperature dependence of lattice parameters indicate weak anomaly around 150 K, temperature below which satellite reflections are observed as shown in Fig. 1 & S4. The corresponding symmetry breaking from orthorhombic to monoclinic is associated with the appearance of the Bragg reflections due to the loss of the 2_1 screw axes in the incommensurate phase Fig. S5. All these structural observations were reproducible on different crystals of different batches, as well as on different X-ray diffraction experiments (in the laboratory or at the Synchrotron Soleil).

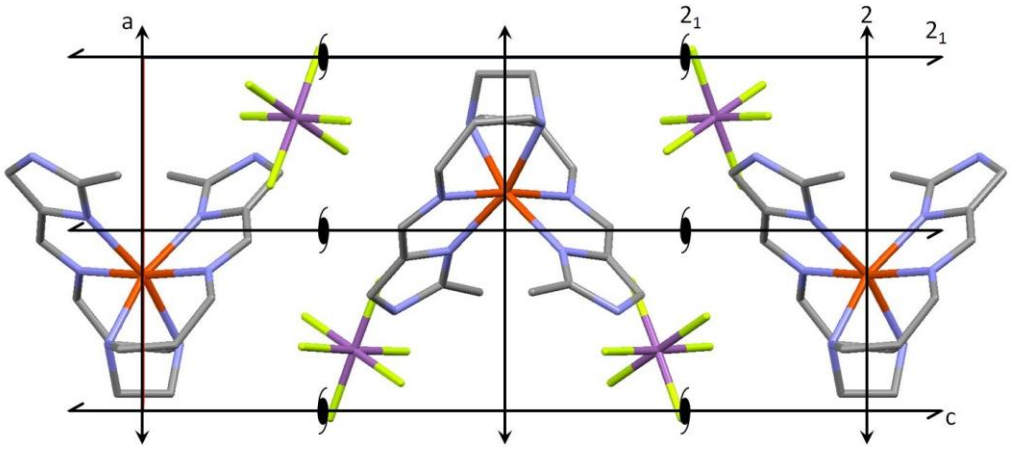

Figure S3. Projection of the crystal packing of the $[Fe^{II}H_2L_2^{-Me}][SbF_6]_2$ complex in the HS phase at 250 K in the (*a*,*c*) plane. H atoms are omitted for clarity. This crystalline structure is isostructural to the one of the $[Fe^{II}H_2L_2^{-Me}][PF_6]_2$ and $[Fe^{II}H_2L_2^{-Me}][AsF_6]_2$ complexes[25,26].

Structure	250 K	140 K	80 K	15 K	15 K 532 nm
Fe-N_1	2.175(3)	2.133(3)	2.089(3)	2.086(3)	2.171(3)
Fe-N_2	2.185(3)	2.149(3)	2.099(3)	2.094(3)	2.203(3)
Fe-N_3	2.214(3)	2.154(3)	2.110(3)	2.112(3)	2.203(3)
<Fe-N_i>	2.191(3)	2.145(3)	2.099(3)	2.097(3)	2.192(3)
γ_{HS}	1.00	0.75	0.52	0.51	1.0

Table S3. Relevant coordination bond lengths [Å], for $[Fe^{II}H_2L^{2-Me}](SbF_6)_2$ at 250 K, 140 K, 80 K, 15 K and in the photoinduced phase at 15 K (532nm). γ_{HS} is deduced from the <Fe-N> bond variation. A similar variation is also observed in the PF_6 and AsF_6 derivatives, between the HS ($<Fe\text{-}N>_{HS} \approx 2.19$ Å) and the LS states ($<Fe\text{-}N>_{LS} \approx 2.01$ Å) with:

$$<Fe\text{-}N>(T)=\gamma_{HS}(T) \times <Fe\text{-}N>_{HS} + (1-\gamma_{HS}(T)) \times <Fe\text{-}N>_{LS}$$

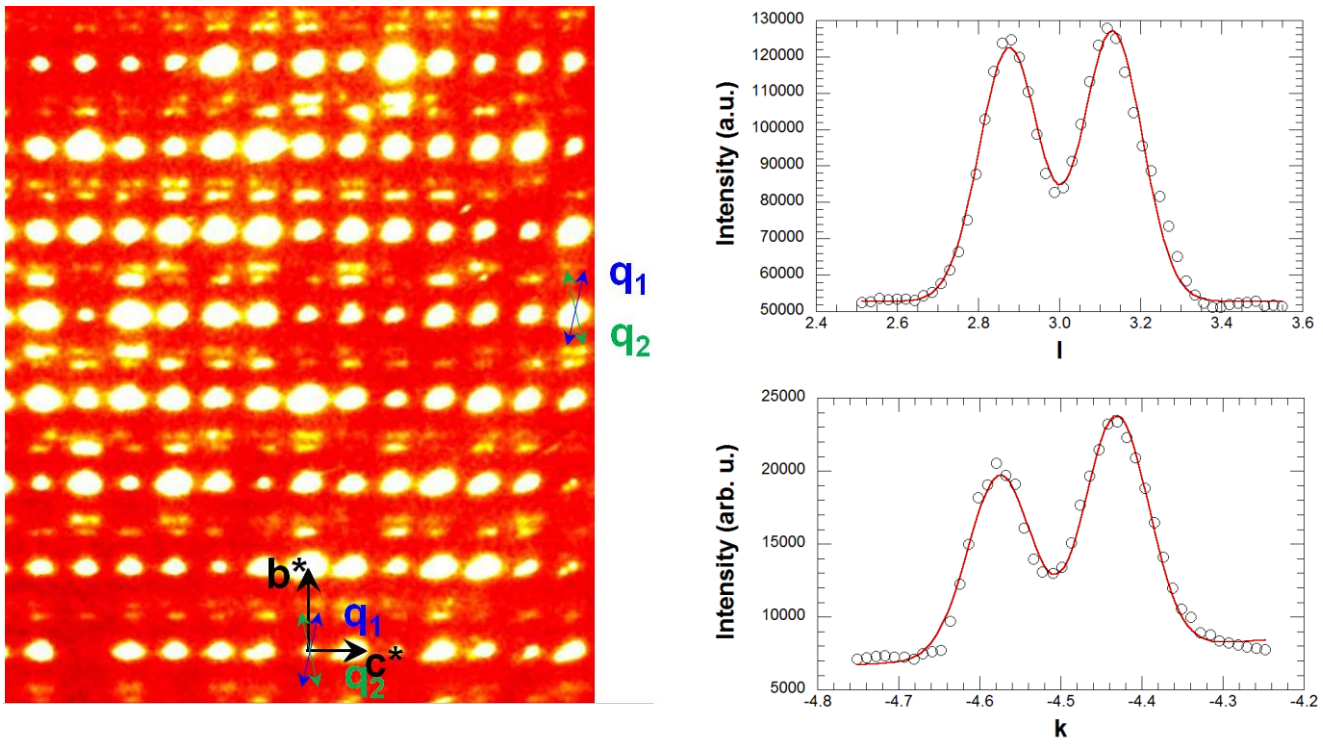

Figure S4: Satellites reflections observed at 80 K in the h=2 reciprocal plane (left), indexed with vector **Q**=h **a*** + k**b*** + l**c*** + m $\mathbf{q_1}$, **or Q**=h **a*** + k**b*** + l**c*** + m $\mathbf{q_2}$ with $\mathbf{q_1}=\beta\mathbf{b}^* + \gamma\mathbf{c}^*$ or $\mathbf{q_2}=-\beta\mathbf{b}^* + \gamma\mathbf{c}^*$. The values β= 0.431(5) and γ=0.131(5) were determined by a least square refinement of the position of several satellites along the **c*** and **b*** directions. Two examples of intensity profiles (right) along **c*** around (2 3.57 3) and **b*** and (2 -4.5 1) are presented: the points are experimental data and the lines the results of the refinements.

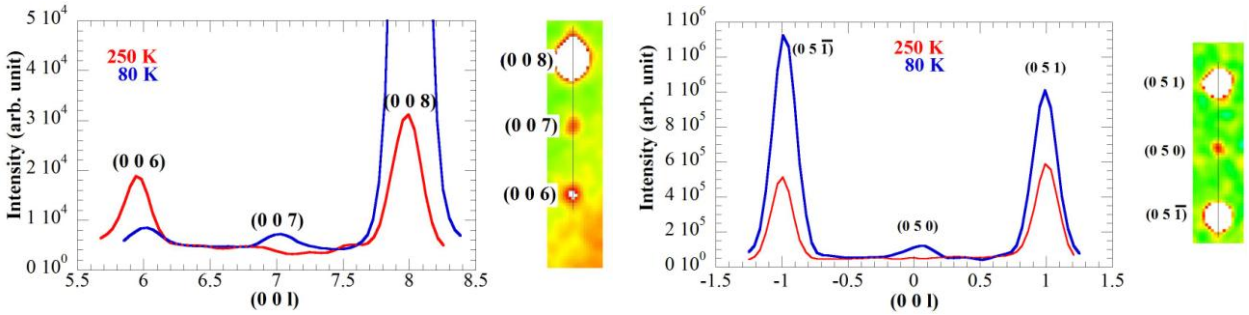

Figure S5. Temperature dependence of the diffracted intensity in the reciprocal space, showing the appearance of the (0 0 7) and (0 5 0) Bragg reflections in the low temperature incommensurate phase characterizing the loss of 2_1 screw axes along **c** and **b** directions respectively.

Superspace description of the incommensurate structure of $[Fe^{II}H_2L^{2\text{-}Me}][SbF_6]_2$.

The structure of the title compound was refined in (3+1)-dimensional superspace. First, the reflection intensities including satellites were integrated using the program CrysAlis[28]. The satellite reflections are extremely weak. Out of 12260 integrated satellites only 677 were observed at the level of 3σ. The structure model was constructed and refined using the computer program Jana2006[31]. The only superspace group compatible with the direction of the q-vector and with loss of the 2_1 screw axes along **b** and **c** is P211(0βγ). Ideally, the structure should be modelled as an occupational modulation of two forms of the molecule – the HS and LS state. However, the intensities of the satellites are too weak to permit a refinement that would refine directly the occupancy of the two forms and the variation of the molecule's geometry. Instead, only the modulation of the atomic positions was refined, and we made use of the known correlation between <Fe-N> and the occupancy of the HS and LS state. Further complication comes from the fact that the satellite reflections are really extremely weak compared to the main reflections. Refining together the basic structure and the modulation parameters resulted in unrealistic modulation parameters. Therefore a two-step procedure was used. First, the average structure was refined against main reflection only and with isotropic atomic displacement parameters (ADP) for the 42 atoms non-H atoms, with 165 parameters including scale factor, 3×40 coordinates of all non Fe atoms, 2 coordinates (x) for the Fe atoms lying on 2 fold axis and 42 isotropic ADP. Then the parameters of the average structure were fixed, and only the modulation parameters of all atoms were refined against both the main and satellite reflections. As only satellites of order 1 were observed, only one harmonic modulation wave was refined for each atom. In this way the structure could be refined to a stable result with 247 parameters including scale factor and 246 modulation parameters. For the 40 non Fe atoms sinus and cosines component of the modulation along x,y,z were refined. Only cosines component modulation parameters are symmetry-allowed for the 2 Fe atoms which are lying on 2 fold axis. Basic refinement characteristics are summarized in Table S4.

Table S4:

Basic parameters of the modulated structure refinement (with 3σ threshold for the observed reflections).

Total number of reflections (all/main/satellites)	24883 / 8481 / 16402
Rint obs (all/main/satellites)	1.99 / 1.86 / 21.53
Indep. observed reflections (all/main/satellites)	6435/ 5758 / 677
Indep all reflections (all/main/satellites)	18664 / 6404 / 12260
Robs [%] (all/main/satellites)	5.36 / 5.06 / 16.68
Rall(all/main/satellites)	13.17 / 5.60 / 47.78
Goodness of fit (obs/all)	2.00/1.44
Refined parameters of the basic structure	165
Refined modulation parameters	247

The number of observed satellite reflections (677 with $I>3\sigma$) seems to be too low to refine the modulation parameters. However, the total number of satellites in the dataset (12260) is very large, and these reflections, although very weak, do contain some structural information (there are 2356 satellites with $I>2\sigma$). It would be possible to limit the number of refined parameters by modulating only the heavy atoms and the atoms close to the iron sites. However, such limitation could bias the resulting modulation amplitudes of the refined atoms. Therefore, we decided to refine modulations of all atoms. In the course of the structure refinement we tested several other scenarios, and they all result in very similar characteristics of the model. This fact and the analysis presented in the next paragraph are good indicators that the information contained in the satellites was enough to reliably determine the basic features of the modulated structure.

The single symmetry-independent molecule of the high-temperature space group $P22_12_1$ (Fig. S3) splits into two independent molecules in the superspace group $P211(0\beta\gamma)$ with central Fe atoms labelled Fe1 and Fe2. Since the molecules lies on a two-fold axis, there are 3 independent N atoms (N1-N3) around each Fe, equivalent to the 3 others (N1'-N3'). The equivalent Ni/Ni' atoms do not have identical modulations, only symmetry equivalent modulations phase shifted by the different atomic coordinates. Fig. S6 shows the dependence of the Fei-Ni and Fei-Ni' distances on the superspace coordinate x_4 for each of the six N atoms around Fe1 and Fe2. As the molecules still lie on a two-fold axis, the bond-length modulation functions, corresponding to occupation modulation functions of the spin-states that we could not refine directly, must be even and the results of the refinement are close to this. For a physically meaningful model resulting from the occupation modulation of HS and LS states, the variation of the 6 Fe-N distances on the same molecule should have the same phase, i.e. either all six N atoms are far from the central iron (HS state), or all six are close (LS state). Figure S6a and 6b shows that this is indeed very well fulfilled. The fact that no constraints on the relative phases were used in the refinement, and still all the modulation functions have very similar phases is the proof that the refined model is in its basic characteristics correct. The amplitude of the Fe-N bond lengths observed here (Fig. S6) are within the 2.0-2.2 Å range typically reported in the literature between LS and HS states. But these 6 independent bonds of the $[Fe^{II}H_2L^{2\text{-}Me}]^{2+}$ cations can have different contractions, as observed in PF_6 and AsF_6 salts.[25,26] However, the variability of the refined amplitudes in the present SbF_6 compound is the demonstration of the limits of the accuracy of the refinement, given by the weakness of the satellites reflections. Therefore, we also refrain from a complete crystallographic analysis, and use the refinement result only to confirm the proposed structure model and to estimate the amplitude of the occupational modulation.

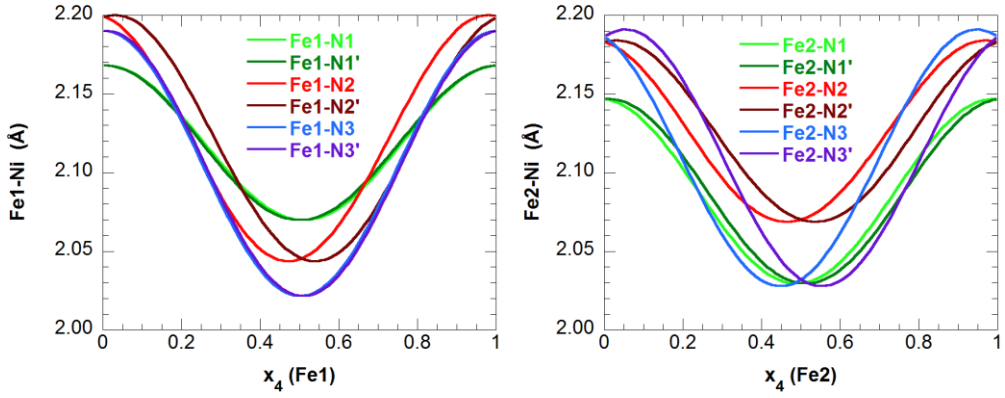

Figure S6: Modulation of the Fe-N distances on the superspace coordinate x_4 around the two symmetry-independent iron atoms of the modulated structure for site 1 (left) and site 2 (right).

These apparent distance modulation curves should be understood as caused by the modulation of the HS population, which is the symmetry breaking order parameter. Averaging the Fe-N distances around Fe1 and Fe2 (Fig. S7, where the N1 atom was excluded as an obvious outlier) and using the relationship between γ_{HS} and <Fe-N> (Table S3) yields the modulation of γ_{HS} on the superspace coordinate x_4 (Fig. 4). The overall average amplitude on Fe1 and Fe2 sites point to a modulation of γ_{HS} around the average value of 0.51, modulated between 0.13 and 0.88.

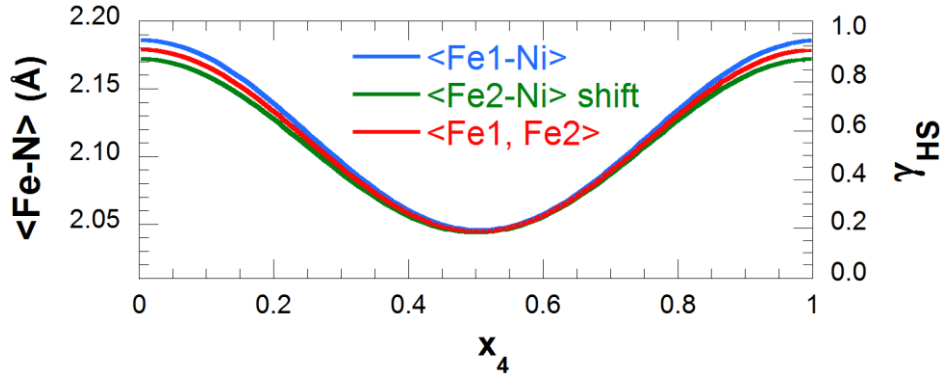

Figure S7: Variation along the superspace coordinate x_4 of the <Fe-N> on Fe1 and Fe2 sites and the averaged value <Fe1, Fe2>. <Fe-N> is scaled on γ_{HS} by using the relation presented in table S3.

References:

28 CrysAlis Pro , Oxford Diffraction Ltd, Version 1.171.35.11, 2012.

29 A. Altomare, M. C. Burla, M. Camalli, G. Cascareno, G. Giacovazzo, A. Guagliardi, A. G. G. Moliterni, G. Polidori, R. Spagna, *J. Appl. Crystallogr.* **32**, 115-119 (1999).

30 G. M. Sheldrick, SHELXL-97, Program for the refinement of crystal structures from diffraction data, University of Göttingen, Germany, 1997.

31 V. Petricek, M. Dusek, & L. Palatinus. (2006). JANA2006. Institute of Physics, Praha, Czech Republic.